The Alignment Effect of Brightest Cluster Galaxies in the SDSS

R.S.J. Kim[1,2], J. Annis[3], M.A. Strauss[1], R.H. Lupton[1], N.A. Bahcall[1], J.E. Gunn[1], J.V. Kepner[1,4], M. Postman[5] for the SDSS collaboration

[1] *Princeton University Observatory, Princeton, NJ 08544, USA*

[2] *Department of Physics and Astronomy, The Johns Hopkins University, 3701 San Martin Dr, Baltimore, MD 21218, USA*

[3] *Fermilab, Batavia, IL 60510, USA*

[4] *MIT Lincoln Laboratory, Lexington, MA 02420, USA*

[5] *Space Telescope Science Institute, 3700 San Martin Dr., Baltimore, MD 21218, USA*

Abstract. One of the most vital observational clues for unraveling the origin of Brightest Cluster Galaxies (BCG) is the observed alignment of the BCGs with their host cluster and its surroundings. We have examined the BCG-cluster alignment effect, using clusters of galaxies detected from the Sloan Digital Sky Survey (SDSS). We find that the BCGs are preferentially aligned with the principal axis of their hosts, to a much higher redshift ($z \gtrsim 0.3$) than probed by previous studies ($z \lesssim 0.1$). The alignment effect strongly depends on the magnitude difference of the BCG and the second and third brightest cluster members: we find a strong alignment effect for the dominant BCGs, while less dominant BCGs do not show any departure from random alignment with respect to the cluster. We therefore claim that the alignment process originates from the same process that makes the BCG grow dominant, be it direct mergers in the early stage of cluster formation, or a later process that resembles the galactic cannibalism scenario. We do not find strong evidence for (or against) redshift evolution between $0 < z < 0.45$, largely due to the insufficient sample size (< 200 clusters). However, we have developed a framework by which we can examine many more clusters in an automated fashion for the upcoming SDSS cluster catalogs, which will provide us with better statistics for systematic investigations of the alignment with redshift, richness and morphology of both the cluster and the BCG.

1 Introduction

There has been an increasing number of reports in the past two decades of coherent orientation between galaxies, clusters and large-scale structure (see Djorgovski 1986 for review). In particular, Bingelli (1982) reported the two very significant alignment signals, both of which were later nick-named the "Bingelli Effect". With 44 low redshift Abell clusters ($z < 0.1$), he reported a significant tendency for (i) neighboring clusters to *point towards each other*, and (ii) the Brightest Cluster Galaxies (BCG) to be aligned with their parent cluster orientations. The first Bingelli effect (cluster-cluster) was later re-investigated, and some confirmed the effect (Rhee & Katgert 1987, West 1989), while others did not (Struble & Peebles 1985). On the other hand, evidence for the second Bingelli effect (BCG-cluster) has been growing steadily over the last two decades. Such studies have involved rich Abell clusters (Struble & Peebles 1985), poor groups of galaxies (Fuller, West, & Bridges 1999) and a full three-dimensional analysis of the Virgo cluster (West & Blakeslee 2000).

However, all BCG-cluster alignment studies to date only probe the phenomenon at low redshifts ($z \lesssim 0.1$), where most of the Abell clusters available for such studies live, typically including a handful of clusters. Studying the BCG alignment effect as a function of redshift with a large sample of clusters is crucial to draw any conclusions on the formation process of the BCGs and the origin of their alignment effect. In this paper, we examine the BCG alignment effect in a sample of 300 clusters of detected by two or more methods in the Sloan Digital Sky Survey (York *et al.* 2000; SDSS), in a redshift range $0.04 \lesssim z \lesssim 0.5$. In the process of this work, we develop a framework with which we can analyze a much larger set of upcoming SDSS cluster samples in an automated fashion; a complete study will be presented in a forthcoming paper (Kim *et al.* 2001d). Throughout this paper, we use $H_0 = 70 \mathrm{km\ s^{-1} Mpc^{-1}}$ and a cosmology in which $\Omega_m = 0.3$ and $\Omega_\Lambda = 0.7$.

2 Defining the Cluster Sample

2.1 Data

The SDSS imaging data is taken with an imaging camera (Gunn *et al.* 1998) on a wide-field 2.5m telescope, in five broad bands (u, g, r, i, z). The point source magnitude limit is $r^* \approx 22.5$ at $1.5''$ seeing (see York *et al.* 2000, Stoughton *et al.* 2001 for more details). The SDSS imaging runs 752 and 756 are equatorial scans that are a part of the Early Data Release (Stoughton *et al.* 2001), and amounts to 230 deg^2 of contiguous area. We use approximately half of this area, 113 deg^2 enclosed by the coordinates $145° < \mathrm{RA} < 190°$ and $-1.25° < \mathrm{DEC} < 1.25°$ for our present study. The median seeing FWHM was 1.4" in Run 752, and 1.3" in Run 756. We construct a galaxy catalog to $r^* = 21.5$ using star-galaxy classification by the SDSS photometric pipeline (`photo`; Lupton *et al.* 2001).

2.2 Cluster Sample Selection

We use three automated cluster finding algorithms for selecting our sample of clusters in the SDSS: two Matched Filter (MF) algorithms, the Hybrid MF (HMF; Kim *et al.* 2001b, hereafter Paper I), the Adaptive MF (AMF; Kepner *et al.* 1999), and the MaxBCG algorithm of Annis *et al.* (2001). The MF techniques select clusters in 2D data by finding peaks in a cluster likelihood map, generated by convolving the galaxy distribution with a matched filter constructed from a model cluster profile and luminosity function. Both MF techniques are outlined in Paper I, and have been applied to the SDSS imaging data in Kim *et al.* (2001c). The MaxBCG technique identifies most likely BCGs based on their well studied characteristics in color-magnitude (c-m) space, and then searches in their vicinities for galaxies with the colors and magnitudes of likely cluster members (i.e., the red-sequence), to determine the presence of a cluster. Due to the limited space provided, we shall refer to Paper I, Annis *et al.* (2001), for the details of these methods (see also Kim *et al.* 2001a).

In order to minimize false positives and select a robust sample, we take only those clusters that are detected by both the MaxBCG and either of the MF methods. The MaxBCG selects clusters with very restrictive color properties, but no constraint is put on the cluster luminosity function or the density profile, while the MF algorithms use the latter criteria exclusively; the two methods are practically orthogonal in their selection criteria. Therefore, combining the two makes our cluster selection especially robust. We obtain 300 clusters with estimated redshifts out to $z \sim 0.55$ in 113 deg^2 (see Kim *et al.* 2001a,d for details). The MaxBCG is particularly useful since it identifies the most likely BCG of each cluster, although not always correctly; in order to flag these incorrect BCG identifications we start by inspecting the 300 cluster candidates by eye. Visual inspection effectively allows us to confirm the identity of the cluster candidate, and to locate the BCG when it is dominant, being either a giant elliptical or a cD with an extended envelope. Each cluster candidate was carefully examined, and was selected if the BCG was visually unambiguous *and* was correctly located by the MaxBCG. We also rejected clusters that had two or more dominant galaxies. This eliminates half of our sample, with a total of 144 clusters remaining. We call this sample "VC" (Visually Confirmed).

We also perform an automated procedure that carries out a similar task of filtering out clusters with likely spurious BCG detections. We inspect the area in c-m space bound with $(g - r)_{bcg}{}^{+0.2}_{-0.1}$ and $r_{bcg}{}^{+0}_{-1}$, where $(g - r)_{bcg}$ and r_{bcg} are the color and magnitude of the detected BCG. If there is any galaxy in the above area, within $0.5\ h^{-1}$ Mpc of the detected BCG, then we reject this cluster since there is a good chance that this brighter galaxy is the true BCG. This eliminates 89 candidates out of the 300 in our initial sample; of these, only 10 out of the 89 had been previously accepted as good candidates by visual inspection. We call the resulting 211 cluster sample "MC" (Machine Confirmed).

2.3 The Degree of "Dominance"

The VC sample does not include clusters in which the BCG is not dominant and therefore not readily identifiable. However, a cluster will always have a brightest member regardless of how dominant it is, all of which are included in the MC sample as long as the BCG is correctly identified. We quantify this "degree of dominance" by the magnitude difference between the BCG (m_1) and the average of the second (m_2) *and* the third (m_3) brightest member: $m_{(1-2,3)} \equiv (m_2 + m_3)/2 - m_1$. The average of m_2 and m_3 is slightly more robust to background contamination than is m_2, it also deweights the fact that there can be two dominant galaxies far more luminous than the rest of the cluster population.
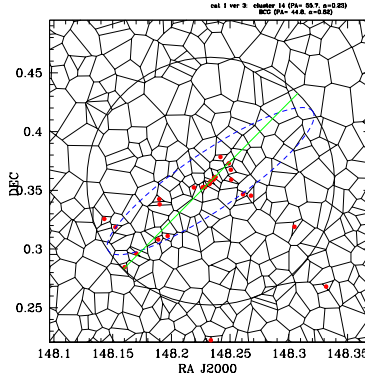
Figure 1: Determining the cluster position angle. Voronoi Tessellation is performed on c-m selected galaxies. The dots represent galaxies with high density contrast, with which we compute ϕ and α. These parameters are represented by the dashed ellipse around the BCG with its major axis normalized to $1h^{-1}$ Mpc (solid circle). The solid line represents the PA of the BCG. This cluster is at z=0.24.

3   Method and Analysis – Shape and Orientation

The orientation and ellipticities of individual BCGs are taken from the outputs of `photo`: the position angle ϕ_{deV} and axis ratio α_{deV} are the parameters of the best fit 2-D de Vaucouleurs law model (Lupton et al. 2001). The shape and orientation of the clusters are measured through a process very similar to detecting clusters with the Voronoi Tessellation Technique (VTT) which is detailed in Paper I (§2.2). The VTT is invoked reversely in order to retreive the cluster members with which we calculate the position angle and ellipticity of the cluster. For each cluster, we apply c-m cuts on all galaxies around the detected BCG (Paper I, Eq. (9)-(11)), which selects a generous set of galaxies whose colors and magnitudes resemble the cluster members. We then apply a Voronoi Tessellation on these galaxies to select those residing in the densest environments as a tracer for typical cluster members: galaxies with $\delta \equiv (\rho - \langle\rho\rangle)/\langle\rho\rangle > 3$ within $1h^{-1}$ Mpc of the BCG, where ρ is the inverse of the Voronoi cell area. We call the final number of selected galaxies, N_{cc}. We then calculate the inverse-radius weighted moments of these galaxies using the BCG as the center ($\mathbf{x'} = \mathbf{x} - \mathbf{x_{bcg}}$), and obtain the Stokes parameters whose relation to the position angle (ϕ) and axis ratio ($\alpha = b/a$) are as follows,

$$Q \equiv \frac{1-\alpha}{1+\alpha}\cos 2\phi = \langle\frac{x'^2}{r^2}\rangle - \langle\frac{y'^2}{r^2}\rangle = 2\langle\frac{x'^2}{r^2}\rangle - 1 \tag{1}$$

$$U \equiv \frac{1-\alpha}{1+\alpha}\sin 2\phi = 2\langle\frac{x'y'}{r^2}\rangle . \tag{2}$$

As with individual BCGs, when a cluster is close to being round, the determination of the orientation becomes noisy and less meaningful. Eqs. (1) and (2) show that the axis ratio α is directly related to the distance from the center of the Q, U plane ($D \equiv \sqrt{Q^2 + U^2}$), $\alpha = (1 - D)/(1 + D)$. When $D = 0$ the object is round, and becomes flatter as $D \to 1$. Thus, clusters with $(Q, U) = (0, 0)$ less than 1σ away are consistent with being round. This translates to $\chi^2 \equiv (Q/\sigma_Q)^2 + (U/\sigma_U)^2 \leq 2.3$ (Press et al. 1992), where σ_Q, σ_U are the shot noise errors on Q, U. We eliminate all clusters that either (a) have BCGs with $\alpha_{deV} > 0.9$, (b) are *consistent with being round*, (c) have member galaxies $N_{cc} < 5$. Each condition reduces the sample size about 20%, leaving altogether 88 clusters in the VC sample, and 115 clusters in the MC sample (for the latter we also limit $z \leq 0.45$). We show an example of a cluster with a well determined position angle and a strongly aligned BCG in Figure 1.

4   Results

We divide the 115 clusters in the MC sample in two separate groups according to their "degree of dominance" measured by the index $m_{(1-2,3)}$ (§2.3): 66 clusters with $m_{(1-2,3)} \geq 0.65$ (MC sample I) and 49 clusters with $m_{(1-2,3)} < 0.65$ (MC sample II). We first present results for MC sample I, the cluster sample with dominant BCGs. Fig. 2a shows the binned distribution of $\Delta\phi$ for all 66 MC
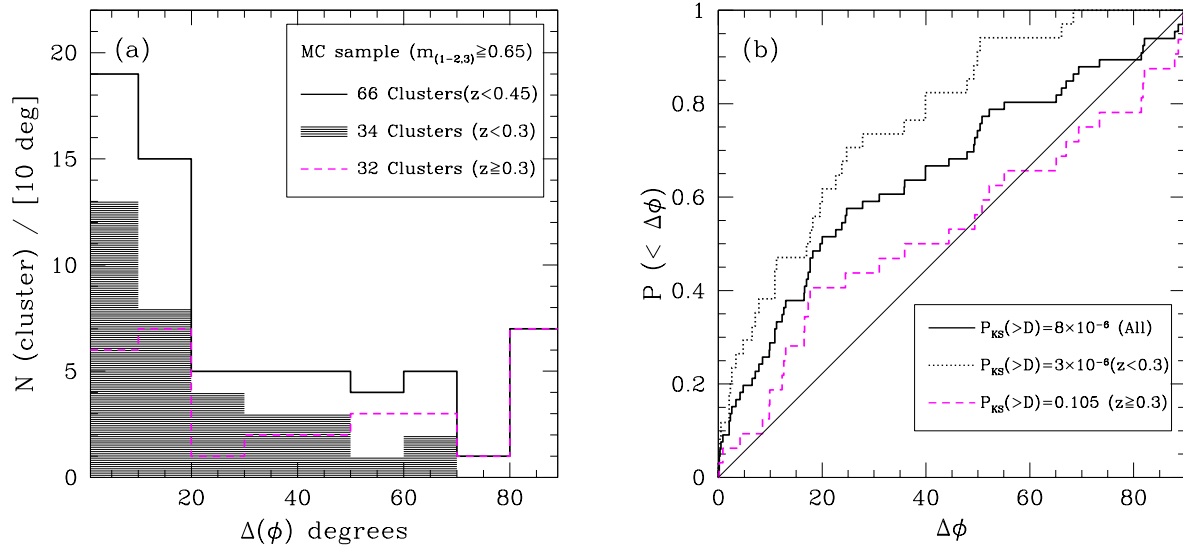
Figure 2: Histogram distribution of the difference in the position angles of the BCG and the cluster, for 66 Machine Confirmed clusters with dominant BCGs (MC sample I; solid-line). The same for 34 low z clusters with $z < 0.3$ (shaded) and 32 high z clusters with $z \geq 0.3$ (dashed-line). (b) Cumulative probability distribution (CPD) of the 66 MC sample I clusters (solid), the 34 low z (dotted), and 32 high z clusters (dashed). All three distributions are significantly different from a random distribution, showing an alignment signal at a high confidence level.

sample I clusters (solid-line). Roughly half (34) of the total sample is confined within $\Delta\phi = \pm 20°$, where one would have expected only 14.7 clusters for a random distribution. This would imply that the number of clusters within $\Delta\phi = \pm 20°$, is more than 3σ above the expected average in a random case. We further split the sample into two redshift ranges, $z < 0.3$ and $z \geq 0.3$, whose distribution of $\Delta\phi$ is also shown in Fig. 2a. Note the striking signal especially at low z (shaded). When comparing these two subgroups, there are hints towards a possible redshift evolution, however, they may well be due to noisier data at higher z and we will not draw any conclusions regarding a redshift evolution, mainly due to the small sample size. The cumulative distributions (unbinned) of $\Delta\phi$ are shown in Figure 2b. The three curves are for: all 66 (solid), 34 low z (dotted) and 32 high z (dashed) MC sample I clusters. K-S tests show that the alignment signals for the 66 clusters and the 34 low z clusters are indeed significant at more than 99.999% confidence, while the high z cluster sample show only a mild correlation at a 90% significance. Although the results for the VC sample with 88 clusters are not shown in this proceeding, they are remarkably similar to the results for the MC sample I (dominant BCGs) shown in Figure 2. K-S statistics indicate that the total VC sample and 46 low z clusters, both show strong alignments at 99.996% and 99.96% confidence levels, and the 42 high z clusters although to a lesser extent, at 95%. The fact that the VC sample results coincide with those of the MC sample I confirms the validity of our automated method for choosing a cluster sample with dominant BCGs.

Finally, the 49 clusters with less dominant BCGs (MC sample II) show an entirely different result. Figure 3 shows the same as Figure 2 for the MC sample II. The alignment signals have totally vanished, and all three curves in Figure 3b have distributions consistent with being random. In particular, the $\Delta\phi$ of all 49 clusters (solid) is consistent with a random distribution at a 82% significance level, well above 1σ ($= 32\%$). The $\Delta\phi$ of the low and high z subsamples are also consistent with a random distribution at 27% and 34% significance ($\sim 1\sigma$). Such absence of the alignment signal is quite remarkable when compared to the strong signal seen for the dominant BCGs.

5   Discussion

Currently, the most favored theory for the origin of the BCG-cluster alignment effect is the anisotropic infall of galaxies that merge to produce BCGs that echo the preferred direction of cluster collapse (Dubinsky 1998, Fuller, West & Bridges 1999). Prompted by predictions of filamentary structures
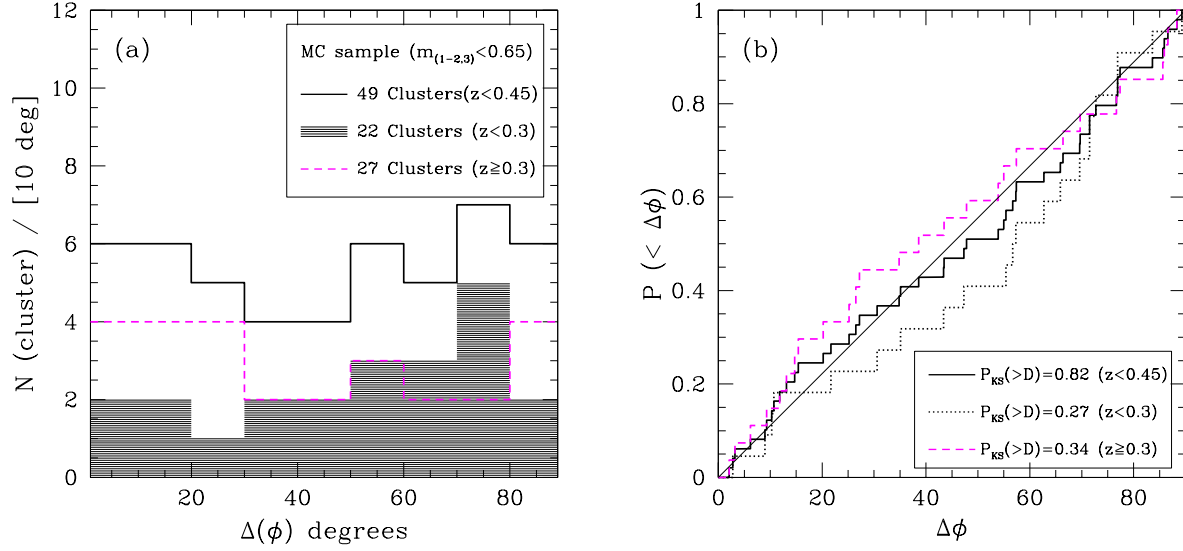
Figure 3: Same as Fig. 2, for total 49 MC clusters with less dominant BCGs selected by $m_{(1-2,3)} < 0.65$, and $z < 0.45$ (MC sample II). The distribution of these 49 clusters does not show any departure from randomness whatsoever ($P_{KS}(> D) = 0.82$). The low and high z subsamples are also consistent with a random distribution within 1σ ($P_{KS}(> D) = 0.27$ and 0.34 for low z and high z, respectively).

being a generic feature of hierarchical structure formation models with Gaussian initial conditions (Bond, Kofman, Pogosyan 1986, Weinberg & Gunn 1990), this picture portrays clusters forming through the infall of material along the filaments, which would tend to align clusters with the nearby large scale structure (van Haarlem & van de Weygaert 1993). Similarly, the formation of the central BCG would have likely undergone anisotropic infall of galaxies as well, assuming that they *are* merger remnants. Indeed, numerical simulations of galaxy collisions have successfully reproduced a prolate de Vaucouleurs–like merger product aligned with the initial collision trajectory, both with individual galaxy collisions (White 1978) and cluster collapses in a cosmological context (Dubinski 1998).

The core result of our work is: (i) we have confirmed the alignment effect of BCGs with their parent clusters seen at low redshifts ($z < 0.1$), to a much higher redshift ($z > 0.3$), and (ii) only the dominant BCGs show such alignments while clusters with less dominant BCGs do not. The first result supports the view that dominant BCGs have relatively early origins, since the dominant BCGs in clusters are aligned with their parent clusters already at a redshift of $z \gtrsim 0.3$. The second result, however, at face value, would naturally seem to fit in the galactic cannibalism scenario (Ostriker & Tremaine 1975): dominant BCGs grow by accreting nearby bright galaxies, making the magnitude difference between the BCGs and their surroundings increase with time. In this process the BCG becomes aligned with the surrounding structure, which explains why less dominant BCGs are *not* seen to be aligned with their surroundings. However, the late evolution scenario by galactic cannibalism has well known drawbacks: the total accreted luminosity in the cluster's lifetime falls short (by a factor of several) of the current observed luminosities of typical cDs (Tremaine 1990). Early BCG formation during cluster formation (consistent with hierarchical clustering), will be more efficient in producing such dominant BCGs, through direct mergers of galaxies (head-on collisions) in a preferred direction that can explain the alignment effect. However, this scenario does not explain the existence of so many clusters with not so dominant BCGs at low redshifts ($z < 0.3$); either those clusters are yet in the process of forming, or they have never had a chance to form a dominant BCG at the early cluster formation stage and still never will. The former seems unlikely since the clusters we have selected are by definition those with well evolved galaxies with uniformly red color (E/S0), and the latter would imply that clusters have inhomogeneous origins and fates.

All these possibilities for the origin of BCGs and their alignment effect with their surroundings can only be narrowed down effectively by observing these effects with many more clusters in all possible redshift ranges. Examining the alignment effect or the evolution of $m_{(1-2,3)}$ with cluster richness or BCG morphology can also provide us with vital clues. In our present study, we have established an automated framework to investigate the alignment effect in many more clusters ($> 10,000$) in the

SDSS and will soon be able to characterize the redshift evolution of these effects for a valuable insight into the origin of the brightest cluster galaxies.

References

[1] Annis, J. *et al.* 2001, *in preparation*

[2] Binggeli, B. 1982, A&A, 107, 338

[3] Bond, J. R., Kofman, L., & Pogosyan, D. 1996, Nature, 380, 603

[4] Djorgovski, S. 1986, *Nearly Normal Galaxies*, pp 227-233, Ed. S. Faber, (New York:Springer)

[5] Dubinski, J. 1998, ApJ, 502, 141

[6] Fuller, T. M., West, M. J., & Bridges, T. J. 1999, ApJ, 519, 22

[7] Gunn, J. E. *et al.* 1998, AJ, 116, 3040

[8] Kepner, J., Fan, X., Bahcall, N., Gunn., J., Lupton, R., Xu, G. 1999, ApJ, 517, 78

[9] Kepner, J. V., & Kim, R. S. J. 2000, submitted to Data Mining and Knowledge Discovery, astro-ph/0004304

[10] Kim, R. S. J. 2001a, Ph.D. Thesis, Princeton University

[11] Kim, R. S. J. *et al.* 2001b, AJ accepted (Paper I), astro-ph/0110259

[12] Kim, R. S. J. *et al.* 2001c, to be submitted to AJ

[13] Kim, R. S. J. *et al.* 2001d, *in preparation*

[14] Lupton, R.H. *et al.* 2001, *in preparation*

[15] Ostriker, J. P., & Tremaine, S. 1975, ApJ, 202, L112

[16] Rhee, G., & Katgert, P. 1987, A&A, 183, 217

[17] Stoughton *et al.* for the SDSS collaboration 2001, *in preparation*

[18] Struble, M. F., & Peebles, P. J. E. 1985, AJ, 90, 582

[19] Tremaine, S. 1990, Dynamics and Interactions of Galaxies, ed. Wielen, pp 394, (NY:Springer)

[20] van Haarlem & van de Weygaert 1993, ApJ, 418, 544

[21] Weinberg, D. & Gunn, J. 1990, MNRAS, 247, 260

[22] West, M. J. 1989, ApJ, 347, 610

[23] West, M. J., & Blakeslee, J. P. 2000, ApJ, 543, L27

[24] White, S. D. M. 1978, MNRAS, 184, 185

[25] York, D. G. *et al.* 2000, AJ, 120, 1579